Petroleum Science 19 (2022) 3016–3028

Contents lists available at ScienceDirect

Petroleum Science

journal homepage: www.keaipublishing.com/en/journals/petroleum-science

Original Paper

Simulation on venting process and valve opening control method for gas trunk pipelines

Li-Li Zuo [a, *], An-Tai Jin [a, b], Qian Chen [a], Qin-Long Dong [c], Yuan-Xin Li [c], Si-Rui Zhao [a]

[a] National Engineering Laboratory for Pipeline Safety/Beijing Key Laboratory of Urban Oil and Gas Distribution Technology, China University of Petroleum (Beijing), Beijing, 102249, China
[b] PetroChina Planning ☐ Engineering Institute, Beijing, 100083, China
[c] National Petroleum and Natural Gas Pipe Network Group Beijing Pipeline Co., Ltd., Beijing, 100101, China

A R T I C L E I N F O

Article history:
Received 7 June 2022
Received in revised form
23 September 2022
Accepted 23 September 2022
Available online 30 September 2022

Edited by Xiu-Qiu Peng

Keywords:
Gas pipeline
Venting time
Transient simulation
Implicit central difference method
Valve Opening Control Method

A B S T R A C T

Determining the venting time of a gas trunk pipeline segment provides an important basis for formulating an emergency plan in the advent of unexpected accidents. As the natural gas venting process corresponds to the transient flow, it is necessary to establish a transient hydraulic-thermal simulation model in order to determine the venting time. In this paper, based on two kinds of venting scenarios in which there is only one venting point in the venting system of a gas trunk pipeline segment—namely, where the venting point is either at one of the two ends or at the junction of two gas trunk pipeline segments—transient hydraulic-thermal simulation models are established. The models consist of gas flow governing equations, the gas state equation, gas physical property equations, initial conditions, and appropriate boundary conditions. The implicit central difference method is used to discretize the gas flow partial differential equations, and the trust-region-dogleg algorithm is used to solve the equations corresponding to each time step, in order to dynamically simulate the whole venting process. The judgment condition for the end of the venting process is that the average pressure of gas trunk pipeline segment is less than 0.11 MPa (actual pressure). Comparing the simulation results of the proposed model with those of the OLGA software and real operational data, we find that the venting time error is less than 10%. On this basis, a venting valve opening control principle is proposed, which prevents the venting noise from exceeded the specified noise value (85 dB) in the venting design of domestic gas pipeline projects. The established calculation model for venting time (dynamic simulation model) for a gas trunk pipeline segment and the proposed opening control principle of venting valve provide reference for the optimal operation of gas pipeline venting systems.

1. Introduction

The natural gas venting system is an important part of gas pipeline stations and valve chambers, guaranteeing the safe and reliable operation of the pipeline. When a gas pipeline is put into production, it is often necessary to carry out natural gas venting operations under emergency response or equipment/facility maintenance scenarios, where the natural gas in the relevant pipeline segments and equipment is vented into the atmosphere through the venting system (Liu et al., 2015; Pu et al., 2014; Li et al., 2019; Ettouney et al., 2012; Soltanieh et al., 2016). In order to formulate a maintenance or emergency response plan that is technically feasible, economically reasonable, and meets HSE requirements, it is required to accurately grasp and reasonably control the venting time and natural gas venting volume of the venting object (e.g., pipeline segment or gas station).

At present, researches about simulation of natural gas pipeline are mainly focused on leakage simulation (Zuo et al., 2015; Chen et al., 2020), supply security and resilience analysis (Su et al., 2022; Zhu et al., 2021), peak shaving and optimization (Chen et al., 2021; Meng et al., 2022), but there are only a few studies focusing on the venting process of gas pipeline. There are three main models for calculating the natural gas venting time for a gas trunk pipeline segment. The first model is based on the assumption that the entire venting flow process is in a critical flow state, where the calculation formula for the venting time is shown in Eq. (1)

* Corresponding author.
E-mail addresses: zuolilicup@163.com, zuolili@cup.edu.cn (L.-L. Zuo).

https://doi.org/10.1016/j.petsci.2022.09.027
1995-8226/

Nomenclature

t	the venting time, s
μ	the valve opening
p_1	the absolute pressure of the gas in the pipeline before venting, MPa
k	the specific heat ratio of natural gas
T	the gas temperature of venting pipe, K
G	the relative density of natural gas
L	the distance of block valves, km
Z	the compression factor
ρ	the gas density, kg/m^3
M	the gas mass flow in the pipe section, kg/ s
λ	the friction coefficient
s	the elevation, m
K	the overall heat transfer coefficient, W/ (m^2 • K)
T_0	the ambient temperature, K
Δx	the space step
M_g	the gas relative molecular mass, kg/kmol
D_i	the J-T effect coefficient of gas, K/MPa
p_{in}	the inlet gas pressures of the resistance element, Pa
K_v	the valve flow coefficient
ρ_{out}	the gas density at the outlet of the resistance element, kg/m^3
Q_{out}	the actual gas volume flow at the outlet of the resistance element, m^3/s
T_{out}	the outlet gas temperatures of the resistance element, K
M_{out}	the outlet gas mass flow of the resistance element, kg/s
$D_{i,out}$	the outlet gas J-T effect coefficient of the resistance element, K/MPa
T_{env}	the ambient temperature, K
p_{env}	the atmospheric pressure, Pa
a	the gas speed of sound, m/s
W_m	the mechanical power, W
U	the gas flow rate at the outlet of the venting riser, m/s
T_0	the atmospheric temperature, K
Ma	the gas Mach number at the outlet of the venting riser
L_p	the sound pressure level at the observed point, dB
r	the distance from the observed point to the outlet of the venting riser (this paper take the value 50 m)
V	the volume of vented pipe segment, m^3
F	the cross-sectional area of venting pipe, m^2
p_2	the absolute pressure of the gas in the pipeline after venting, MPa
R_g	the gas constant, J/(kg·K)
P	the initial pressure of the vented pipe segment, MPa
D	the inner diameter of the vented pipe segment, mm
f	the valve resistance factor
d	the inside diameter of the venting pipe, mm
A	the flow area of the pipe segment, m^2
x	length along the pipeline, m
h	the gas enthalpy, J/kg
g	the gravitational acceleration, m/s^2
T	the gas temperature, K
T_{cp}	the gas temperature, °C
Δt	the time step
R	the gas constant (equal to 8.314 kJ/(kmol • K))
h^0	the enthalpy of the ideal gas, kJ/kg
C_p	the specific constant pressure heat capacity, kJ/(kg·K)
p_{out}	the outlet gas pressures of the resistance element, Pa
ρ_{in}	the gas density at the inlet of the resistance element, kg/m^3
Q_{in}	the actual gas volume flow at the inlet of the resistance element, m^3/s
T_{in}	the inlet gas temperatures of the resistance element, K
M_{in}	the inlet gas mass flow of the resistance element, kg/s
$D_{i,in}$	the inlet gas J-T effect coefficient of the resistance element, K/MPa
T_{ini}	the gas initial temperature of gas trunk pipeline segment, K
p_{ini}	the gas initial pressure of gas trunk pipeline segment, Pa
k_T	the polytropic process index
W_a	the total sound power, W
η	the sound efficiency
ρ_0	the atmospheric density, kg/m^3
K_a	the sound power factor (the value is about 5 * 10^{-5})
L_w	the total sound power level at the outlet of the venting riser, dB
DI	the directivity index (the value is −6 under the subsonic flow and −1 under the critical flow)

(Sichuan Petroleum Design Institute, 1974). As the influence of the non-critical flow state on the venting time during the venting process is not considered, the venting time calculated by this model may be shorter than the actual venting time.

$$t=\frac{V}{\mu F}*\frac{\ln\frac{p_1}{p_2}}{\sqrt{kR_gT\left(\frac{2}{k+1}\right)^{\frac{k+1}{k-1}}}} \tag{1}$$

Another formula for calculating the venting time in a critical flow model is shown in Eq. (2) (Sichuan Petroleum Administration and Southwest Petroleum Institute, 1995). Compared with Eq. (1), this empirical formula considers the resistant effect of the valve on the venting gas, adding a valve resistance factor f.

$$t=\frac{0.191974P_1^{(1/3)}G^{0.5}D^2Lf}{60Zd^2} \tag{2}$$

The second calculation model of the venting time is based on the Fanno equation (Lin et al., 2019; Lou et al., 2014; Bai et al., 2015). The basic idea is as follows: according to the initial pressure p_1 of the gas trunk pipeline segment and the pressure p_0 at the end of the venting process, take a certain micro-pressure decrease value Δp to divide the pressure interval $[p_1, p_0]$ into equal parts $[p_1, (p_1-\Delta p)]$, $[(p_1-\Delta p), (p_1-2\Delta p)]$ and so on. First, we calculate the venting time for the average pressure of the trunk pipeline segment to change in each sub-interval; that is, the time corresponding to the decrease of the average pressure in the pipeline from $p_1 - k\bullet\Delta p$ to $p_1-(k+1)\bullet\Delta p$. The total venting time for the system is equal to the sum of the venting times corresponding to all pressure sub-intervals. In particular, the time that the average pressure of the pipeline takes to change in a sub-interval is equal to the change of the gas volume in the pipe segment during the process divided by the instantaneous venting rate. When calculating the instantaneous venting rate, it is assumed that the thermodynamic process of the gas entering the venting pipe inlet from the trunk pipeline segment is an adiabatic expansion process. The instantaneous venting rate is calculated using friction- and adiabatic-based one-dimensional flow equations (i.e., the Fanno equation, which can be derived from the continuity equation, momentum equation, energy equation, gas state equation, and physical parameter calculation formula (Lin et al., 2019; Lou et al., 2014; Bai et al., 2015; Wei et al., 2021).

The third method involves performing unsteady hydrothermal simulation of the venting process, in order to determine the venting time according to the variation in some simulation parameters (e.g., the flow rate of the venting riser outlet, pressure of the gas trunk pipeline, and so on). In previous research (Liu et al., 2014), the venting process of a gas trunk pipeline segment was simulated based on the unsteady hydraulic thermal simulation model and the characteristic line algorithm, in order to calculate the venting time. The boundary conditions used were that the pressure and temperature of the venting riser outlet were respectively equal to the atmospheric pressure and the ambient temperature, and the temperature of each node of the gas trunk pipeline segment was always equal to the ambient temperature. Through analysis, it was found that the deviation between the venting time calculated using this method and the actual venting time was about 10%. Due to the short venting pipe of the station venting system, in order to ensure the stability of the algorithm, only a short time step (e.g., 0.01s) can be selected when using the characteristic line method, while the venting time of a gas trunk pipeline segment is usually long (e.g., several hours). Therefore, using the characteristic line method to simulate the scene requires a large amount of calculation. In addition, hydraulic—thermal simulation model of gas trunk pipeline segment venting can also be established based on commercial software (e.g., TGNET, HYSYS, OLGA, SPS, and so on) (Qiao et al., 2013; Zhang, 2021; Pei et al., 2014; Jia et al., 2016). As some software, such as SPS and TGNET, do not possess the functionality to simulate the venting process of gas trunk pipeline segments, in previous researches (Xiong et al., 2014; Li et al., 2018), the simulation of the venting process was approximated by simulating leakage or distribution scenarios. As the boundary conditions in leakage or distribution scenarios are inconsistent with the boundary conditions in actual venting scenarios, the simulation results of these software may deviate from the actual situation, to a certain extent. In addition, some simulation software takes a long time to simulate the venting scene (e.g., the time spent by OLGA software to simulate the example in this paper was 27 min), making them difficult to apply for calculation of the venting time in emergency situations.

In summary, calculation models for the venting time based on critical flow or Fanno equation approaches have been simplified, to varying degrees, such that these two models cannot accurately and comprehensively reflect the venting process of a natural gas pipeline segment. Meanwhile, considering methods based on unsteady hydraulic—thermal simulation, the characteristic line method used in the existing literature has low solution efficiency, while commercial software have shortcomings such as an inability to simulate the venting scene equivalently or cumbersome simulation time. Therefore, it is necessary to conduct an in-depth analysis of the venting system and its simulation method for natural gas trunk pipeline segments, in view of the above deficiencies, in order to propose a more applicable and efficient method for simulating the venting process of a natural gas trunk pipeline segment, allowing for accurate calculation of the venting time. There are three main difficulties associated with this problem:

(1) For the venting of a gas trunk pipeline segment, appropriate boundary conditions need to be selected, in order to satisfy the closure of the system of equations.
(2) As the flow rate at the outlet of the venting riser usually cannot exceed the speed of sound, there are two possible conditions for the boundary conditions at the outlet of the venting riser (known pressure or flow rate at the outlet), and switching between the two boundary conditions needs to be considered during simulation.
(3) For the solution algorithm of the simulation model, the simulation efficiency should be improved as much as possible, under the premise of satisfying the solution stability conditions.

In this paper, we propose specific solutions for the above difficulties, and establish a simulation model for the venting of a natural gas trunk pipeline segment. Based on this model, the venting time of the natural gas trunk pipeline segment can be determined. The remainder of this paper is structured as follows: In Section 2, the venting simulation model is introduced, including the general idea of modeling, basic equations, boundary conditions, initial conditions, and simulation logic. In Section 3, a venting example, the simulation results of the corresponding program in this paper, and OLGA simulation results and real operational data are compared and analyzed. In Section 4, based on the established venting simulation model, an opening control method for venting valves is proposed. Section 5 provides our conclusions.

2. Simulation model

2.1. Basic idea

In order to accurately calculate the venting time of a natural gas trunk pipeline segment, in this paper, we consider two kinds of venting scenarios, in which there is only one venting point in the venting system of a gas trunk pipeline segment: the venting point is either at one of the two ends of the segment or at the junction of two gas trunk pipeline segments. Transient hydraulic—thermal simulation models are established for both cases. The models consist of gas flow partial differential equations, the gas state equation, gas physical property equations, initial conditions, and appropriate boundary conditions. As the venting time for a gas trunk pipeline segment is generally long (ranging from tens of minutes to several hours), in order to shorten the simulation time, a slightly larger time step should be selected. Furthermore, to adapt to the short pipeline in the venting system, it is necessary to ensure that the solution method used for the simulation model has good stability. As the implicit central difference method unconditionally satisfies the computational stability, this method is used to discretize the gas flow partial differential equation. Then, we introduce the gas state equation, gas physical property equations, initial conditions, and boundary conditions, ensuring that the mathematical equations corresponding to each time step in the simulation model are closed. Then, we apply a non-linear system of equations solver function to solve the system of equations at each time step in the simulation model. Thus, the dynamic simulation of the entire venting process of the natural gas trunk pipeline segment is realized, and the venting time of the natural gas trunk pipeline segment is obtained, according to the change of the pressure of the trunk pipeline segment (it can be considered that the venting process ends when the actual average pressure in the trunk pipeline segment is lower than 0.11 MPa).

For the two kinds of venting scenarios studied in this paper, the difference mainly lies in the boundary conditions. The gas flow governing equations, the gas state equation, gas physical property equations, and initial conditions of the two models are consistent. Sections 2.2-2.4 introduce the above mentioned general equations, initial conditions, and boundary conditions for the two venting models, respectively. Section 2.5 discusses the closure of the simulation model equations, and details the logic structure of the simulation program.

2.2. Gas flow partial differential equations and implicit differential discrete

The gas flow governing equations include continuity, momentum, and energy equations (Li and Huang, 2016; Chen et al., 2020), as follows:

(1) Continuity equation

$$\frac{\partial \rho}{\partial \tau}+\frac{1}{A}\frac{\partial M}{\partial x}=0 \tag{3}$$

(2) Momentum equation

$$\frac{1}{A}\frac{\partial M}{\partial \tau}+\frac{\partial}{\partial x}*\left(p+\frac{M^2}{A^2\rho}\right)+g\frac{ds}{dx}\rho+\frac{\lambda}{2d}\frac{M^2}{A^2}\frac{1}{\rho}=0 \tag{4}$$

(3) Energy equation

$$\frac{\partial}{\partial \tau}\left[\rho\left(h-\frac{p}{\rho}+\frac{M^2}{2A^2\rho^2}\right)\right]+\frac{\partial}{\partial x}\left[\frac{M}{A}\left(h+\frac{M^2}{2A^2\rho^2}\right)\right]+\frac{M}{A}\frac{ds}{dx}g+\frac{4K(T-T_0)}{d}=0 \tag{5}$$

The partial differential Eqs. (3)–(5) can be discretized by the implicit central difference method, which has the advantage of unconditional stability compared with characteristics method (Chaczykowski and Zarodkiewicz, 2017; Elaoud et al., 2017; Helgaker et al., 2014).The discretized equations are:

(1) Continuity equation

$$p_i^{k+1}+\rho_{i+1}^{k+1}-\rho_{i+1}^{k}-\rho_i^{k}+\frac{1}{A}\frac{\Delta t}{\Delta x}\left(M_{i+1}^{k}-M_i^{k}+M_{i+1}^{k+1}-M_i^{k+1}\right)=0 \tag{6}$$

(2) Momentum equation

$$\begin{aligned}&\frac{1}{A}\left(M_i^{k+1}+M_{i+1}^{k+1}-M_{i+1}^{k}-M_i^{k}\right)+\frac{\Delta t}{\Delta x}\left[\rho_{i+1}^{k}+\left(\frac{M_{i+1}^{k}}{A}\right)^2\frac{1}{\rho_{i+1}^{k}}\right.\\&\left.-\rho_i^{k}-\left(\frac{M_i^{k}}{A}\right)^2\frac{1}{\rho_i^{k}}+\rho_{i+1}^{k+1}+\left(\frac{M_{i+1}^{k+1}}{A}\right)^2\frac{1}{\rho_{i+1}^{k+1}}-p_i^{k+1}-\left(\frac{M_i^{k+1}}{A}\right)^2\frac{1}{\rho_i^{k+1}}\right]\\&+\frac{1}{2}\Delta t*g*\frac{ds}{dx}\left(\rho_i^{k+1}+\rho_i^{k}+\rho_{i+1}^{k+1}+\rho_{i+1}^{k}\right)+\frac{\Delta t*\lambda}{4d}\left[\left(\frac{M_{i+1}^{k}}{A}\right)^2\frac{1}{\rho_{i+1}^{k}}\right.\\&\left.+\left(\frac{M_i^{k}}{A}\right)^2\frac{1}{\rho_i^{k}}+\left(\frac{M_{i+1}^{k+1}}{A}\right)^2\frac{1}{\rho_{i+1}^{k+1}}+\left(\frac{M_i^{k+1}}{A}\right)^2\frac{1}{\rho_i^{k+1}}\right]=0\end{aligned} \tag{7}$$

(3) Energy equation

$$\begin{aligned}&\rho_{i+1}^{k}h_i^{k+1}-p_i^{k+1}+\left(\frac{M_i^{k+1}}{A}\right)^2*\frac{1}{2\rho_i^{k+1}}-\rho_i^{k}h_i^{k}+\rho_i^{k}-\left(\frac{M_i^{k}}{A}\right)^2*\frac{1}{2\rho_i^{k}}+\rho_{i+1}^{k+1}h_{i+1}^{k+1}-\rho_{i+1}^{k+1}\\&+\left(\frac{M_{i+1}^{k+1}}{A}\right)^2*\frac{1}{2\rho_{i+1}^{k+1}}-\rho_{i+1}^{k}h_{i+1}^{k}+\rho_{i+1}^{k}-\frac{M_{i+1}^{k}}{A}\Big)^2*\frac{1}{2\rho_{i+1}^{k}}+\frac{\Delta t}{\Delta x}*\left[\frac{M_{i+1}^{k+1}}{A}h_{i+1}^{k+1}+\left(\frac{M_{i+1}^{k+1}}{A}\right)^3*\frac{1}{2\left(\rho_{i+1}^{k+1}\right)^2}-\frac{M_i^{k+1}}{A}h_i^{k+1}\right.\\&\left.-\left(\frac{M_i^{k+1}}{A}\right)^3*\frac{1}{2\left(\rho_{i+1}^{k}\right)^2}+\frac{M_{i+1}^{k}}{A}h_{i+1}^{k}+\left(\frac{M_{i+1}^{k}}{A}\right)^3*\frac{1}{2\left(\rho_{i+1}^{k}\right)^2}-\frac{M_i^{k}}{A}h_i^{k}-\left(\frac{M_i^{k}}{A}\right)^3*\frac{1}{2\left(\rho_i^{k}\right)^2}\right]\\&+\frac{g*\Delta t}{2A}*\frac{ds}{dx}\left(M_i^{k+1}+M_i^{k}+M_{i+1}^{k+1}+M_{i+1}^{k}\right)+\frac{2*K*\Delta t}{d}\left(T_i^{k+1}+T_i^{k}+T_{i+1}^{k+1}+T_{i+1}^{k}-4T_0\right)=0\end{aligned} \tag{8}$$

The right superscripts k and $k+1$ of each variable represent two adjacent time steps, while the right subscripts i and $i+1$ of the variables represent two adjacent spatial steps.

2.3. Gas state equation and physical calculation formula

The BWRS equation was chosen as the gas state equation (Li and Huang, 2016). In order to ensure that the density unit (kmol/m^3) and the pressure unit (kPa) in the gas state equation are consistent with Eqs. (6)–(8), the density and pressure in the original gas state equation were transformed, where the transformed equation is shown in Eq. (9).

$$\begin{aligned}&\frac{\rho}{M_g}RT+\left(B_0RT-A_0-\frac{C_0}{T^2}+\frac{D_0}{T^3}-\frac{E_0}{T^4}\right)\left(\frac{\rho}{M_g}\right)^2\\&+\left(bRT-a-\frac{d}{T}\right)\left(\frac{\rho}{M_g}\right)^3+\alpha\left(a+\frac{d}{T}\right)\left(\frac{\rho}{M_g}\right)^6+\frac{c}{T^2}\left(\frac{\rho}{M_g}\right)^3\\&\left[1+\gamma\left(\frac{\rho}{M_g}\right)^2\right]exp\left[-\gamma\left(\frac{\rho}{M_g}\right)^2\right]-\frac{p}{1000}=0\end{aligned} \tag{9}$$

$A_0, B_0, C_0, D_0, E_0, a, b, c, d, \alpha$, and γ can be calculated according to the gas composition (Li and Huang, 2016).

The gas properties involved in the venting simulation process include the enthalpy of natural gas and the Joule-Thomson (J-T) effect coefficient. Under given temperature and pressure conditions, the enthalpy of the actual gas is equal to the enthalpy of the ideal gas under the conditions plus the isothermal enthalpy difference. The formulas for calculating the enthalpy and isothermal enthalpy difference of an ideal gas are shown in Eqs. (11) and (12), respectively, where the values of the coefficients A, B, C, D, E, F in Eq. (11) and $A_0, B_0, C_0, D_0, E_0, a, b, c, d, \alpha, \gamma$ in Eq. (12) can be found in the literature (Li and Huang, 2016).

$$h = 1000*\left[h^0 + \frac{\left(h - h^0\right)}{M_g}\right] \tag{10}$$

$$h^0 = A + BT + CT^2 + DT^3 + ET^4 + FT^5 \tag{11}$$

$$\begin{aligned} h - h^0 = & \left(B_0RT - 2A_0 - \frac{4C_0}{T^2} + \frac{5D_0}{T^3} - \frac{6E_0}{T^4}\right)*\left(\frac{\rho}{M_g}\right) \\ & + \left(bRT - \frac{3}{2}a - \frac{2d}{T}\right)*\left(\frac{\rho}{M_g}\right)^2 + \alpha\left(\frac{6}{5}a + \frac{7d}{5T}\right)*\left(\frac{\rho}{M_g}\right)^5 \\ & + \frac{c}{\gamma T^2}\left\{3 - \left[3 + \frac{\gamma}{2}\left(\frac{\rho}{M_g}\right)^2 - \gamma^2\left(\frac{\rho}{M_g}\right)^4\right]*exp\left[-\gamma\left(\frac{\rho}{M_g}\right)^2\right]\right\} \end{aligned} \tag{12}$$

The formula for the J-T effect coefficient D_i is shown in Eq. (13), where the specific constant pressure heat capacity C_p of the gas can be calculated according to Eq. (14).

$$D_i = \frac{1}{C_p}\left(\frac{0.98*10^6}{T_{cp}^2} - 1.5\right) \tag{13}$$

$$C_p = \frac{1}{M_g}\left(13.19 + 0.092T - 6.24*10^{-5}T^2 + \frac{1.915*10^{11}*\left(p*10^{-6}\right)^{1.124}M_g}{T^{5.08}}\right) \tag{14}$$

2.4. Boundary and initial conditions

There are generally three types of boundary condition involved in the single-point venting system of a gas trunk pipeline segment.

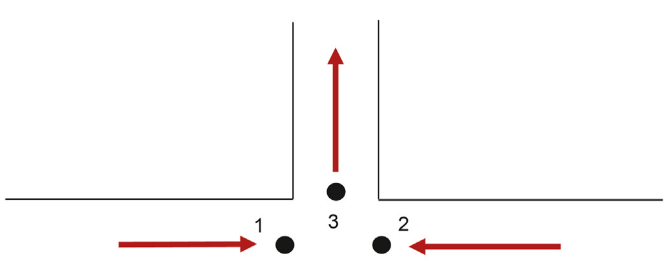

Fig. 1. Schematic diagram corresponding to the boundary conditions at the intersection of gas trunk pipeline segments.

The first type is at the position of the resistance element (e.g., the venting valve), the second type is at the intersection of the gas trunk pipeline segments (e.g., when the venting point is at the junction of the two pipe segments, the intersection of the gas trunk pipeline segment and the venting pipeline), and the third type is the closed end of the shut-off valve and the outlet of the venting riser.

For the first type of boundary condition, we only consider the venting valve as a resistance element in the venting system, and ignore the friction loss at resistance elements such as reducers and elbows. The venting valve must satisfy the pressure drop formula (Zhang, 1994), the temperature drop formula, and the mass flow balance formula, given by Eqs. 15–17:

$$p_{in} - p_{out} = \frac{12.96*10^7}{K_v^2}*g*\left(\frac{Q_{in} + Q_{out}}{2}\right)^2\left(\frac{\rho_{in} + \rho_{out}}{2}\right) \tag{15}$$

$$T_{in} - T_{out} = \frac{\left(D_{i,in} + D_{i,out}\right)}{2}*(p_{in} - p_{out})*10^{-6} \tag{16}$$

$$M_{in} - M_{out} = 0 \tag{17}$$

For the second type of boundary condition, such as the case of the intersection shown in Fig. 1, there are four boundary conditions, described as follows:

(1) The pressure at the junction is equal (including two boundary conditions); that is, $p_1 = p_2$ and $p_2 = p_3$.
(2) The mass flow into the intersection is equal to the mass flow out of the intersection; that is, $M_1 + M_2 = M_3$.
(3) The gas mixing temperature calculation formula, as shown in Eq. (18), is satisfied at the intersection.

$$T_3 = \frac{M_1T_1 + M_2T_2}{M_1 + M_2} \tag{18}$$

The third type of boundary conditions requires the following:

(1) The mass flow at the closed end of the shut-off valve is 0.
(2) The gas state change at the closed end of the shut-off valve is a polytropic process, as shown in Eq. (19). The polytropic process index k_T can be determined according to the initial and final conditions (the final temperature is equal to the ambient temperature, and the final pressure is equal to the atmospheric pressure).

$$\frac{T_{env}}{T_{ini}} = \left(\frac{p_{env}}{p_{ini}}\right)^{\frac{k_T - 1}{k_T}} \tag{19}$$

(3) As the gas flow state of the venting process will go through the states of critical flow and subsonic flow, the boundary condition at the outlet of the venting riser is that the pressure is equal to atmospheric pressure or the flow rate is equal

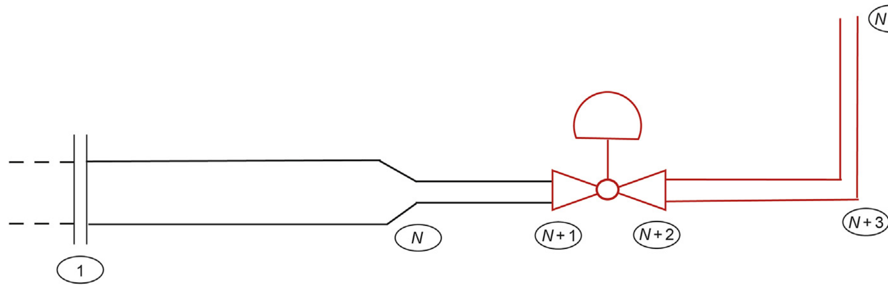

Fig. 2. Schematic diagram for the closure analysis of the system of equations in the single-point venting scenario (the venting point is at one of the two ends).

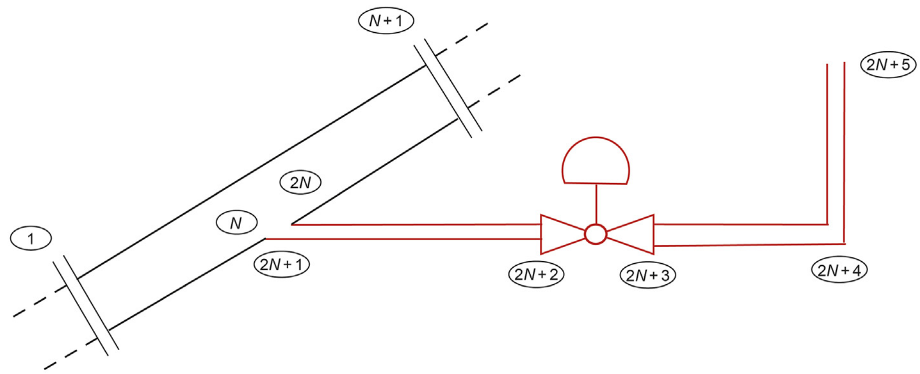

Fig. 3. Schematic diagram for the closure analysis of the system of equations in the single-point venting scenario (the venting point is at the junction of the two gas trunk pipeline segments).

to the local speed of sound. The specific idea is as follows: first, use the outlet pressure equal to atmospheric pressure as the boundary condition. If the calculated outlet velocity is less than or equal to the local speed of sound, the pressure boundary condition is reasonable for the current time step; otherwise, the outlet boundary condition needs to be switched to the outlet velocity equal to the local speed of sound. The speed of sound at the outlet of the venting riser can be calculated according to Eq. (20) (Li and Huang, 2016).

$$a = \sqrt{ZRT} \tag{20}$$

Before venting, the upstream and downstream shut-off valves of the gas trunk pipeline segment must be turned off. As the gas in the trunk pipeline segment usually stabilizes within a short time after the shut-off valves are closed, we assume that the gas in the trunk pipeline segment is stable at the initial time of venting (i.e., the initial mass flow of each node of the trunk pipeline segment is 0, and the initial pressure is equal to the gas equilibrium pressure). For each node of the venting system pipeline downstream behind the venting valve, the initial pressure is equal to the atmospheric pressure and the initial temperature is equal to the ambient temperature.

2.5. Closure analysis and the logical structure of simulation model

The simplified topology diagram of the single-point venting scenario in which the venting point at one of the two ends is shown in Fig. 2. The trunk pipeline segment is divided into $N-1$ sections, the venting pipeline is divided into two small sections (downstream of the gas trunk pipeline segment to the venting valve inlet, and the venting valve outlet to the bottom of the venting riser), the venting riser is regarded as a small segment. The unknowns at each time step in the simulation model are the density ρ, temperature T, mass flow M, pressure p, and enthalpy h of each node, such that there are $5(N+4)$ unknowns in the simulation model at each time step. There are $N+2$ pipe sections in this system, so there are $3(N+2)$ basic pipe flow equations at each time step. For each time step, the gas state equation and enthalpy calculation formula at each node must be considered, including $2(N+4)$ equations. In addition, there are 3 boundary conditions at the venting valve, 2 boundary conditions at the closed end, and 1 boundary condition at the outlet of the venting riser, for a total of 6 boundary conditions. In this venting scenario, the number of equations in the simulation model is equal to the number of unknowns at each time step, so the equations in the simulation model are closed.

The simplified topology diagram of the single-point venting scenario in which the venting point is at the junction of two gas trunk pipeline segments is shown in Fig. 3, where the unknowns at each time step in the simulation model are the density ρ, temperature T, mass flow M, pressure p, and enthalpy h of each node, such that there are $5(2N+5)$ unknowns in the simulation model at each time step. There are $2N+1$ pipe sections in this system, so there are $3(2N+1)$ basic pipe flow equations at each time step. For each time step, the gas state equation and enthalpy calculation formula at each node must be considered, including $2(2N+5)$ equations. In addition, there are 4 boundary conditions at the intersection of gas trunk pipeline segments, 3 boundary conditions at the venting valve, 2 boundary conditions at each closed end, and 1 boundary condition at the outlet of the venting riser, for a total of 12 boundary conditions. Thus, in this venting scenario, the number of equations in the simulation model is equal to the number of unknowns at each time step, so the equations in the simulation model are also closed.

The trust-region-dogleg algorithm can be used to solve the non-linear system of equations at each time step. If the actual average pressure of the gas trunk pipeline segments is lower than 0.11 MPa,

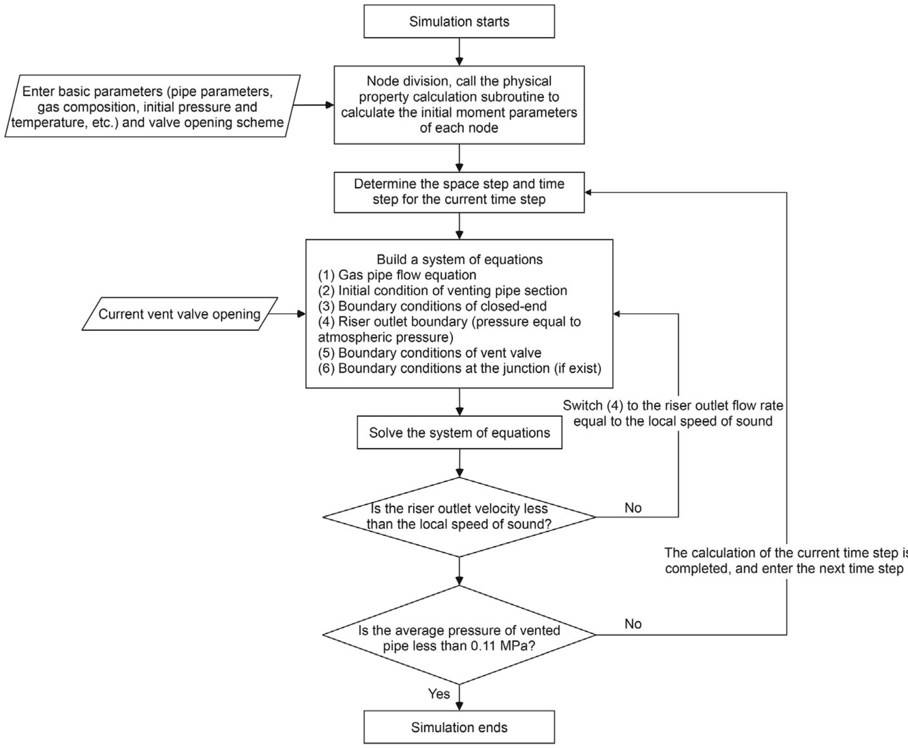

Fig. 4. Logical structure of single-point venting simulation program.

Table 1
Parameters of the gas trunk pipeline segment and venting system pipeline.

	Trunk pipeline	Venting pipeline	Venting riser
Length, m	16,000	6	20
Pipe diameter, mm	660	200	200
Wall thickness, mm	10.3	7.5	7.5
Roughness, mm	0.01	0.46	0.46

Table 2
Gas composition.

Composition	Mole fraction, %
Methane	97.5
Ethane	0.2
Propane	0.2
Nitrogen	1.6
Carbon dioxide	0.5

Table 3
Relationship between the flow coefficient and the opening of the venting valve.

Opening	100	90	80	70	60	50	40	30	20	10	5
Flow coefficient	1000	760	500	350	220	150	110	80	40	20	10

the venting process simulation ends. The logical structure of the single-point venting simulation program is shown in Fig. 4.

3. Case study

3.1. Basic conditions of the example

The basic parameters of the trunk pipeline segments and the venting system pipeline are provided in Table 1, while the gas composition is detailed in Table 2. The initial pressure and temperature of the gas before venting in the trunk pipeline segments were 2.8 MPa and 286 K, respectively. The total heat transfer coefficient of the pipeline was 1.1 $W/(m^2 \bullet K)$. The relationship between the flow coefficient and the opening of the venting valve is shown in Table 3. It was assumed that the opening of the venting valve increased linearly from 0% to 100% from 0 to 5 min. During the simulation, the time step of the simulation was 30 s, the spatial step of the gas trunk pipeline segments was 2 km, and the venting pipeline was divided into two small sections (downstream of the gas trunk pipeline segment to the venting valve inlet, and the venting valve outlet to the bottom of the venting riser). The venting riser was regarded as a small segment.

3.2. Comparison and analysis of simulation results

Based on the model shown in Fig. 2 and the basic conditions in Section 3.1, the proposed method's simulation results and those of the OLGA software are shown in Fig. 5, including the venting riser outlet flow rate, accumulated gas volume flow in standard state, trunk pipeline mid-point pressure, and venting riser outlet pressure. The corresponding venting times with the two simulation methods were 96.5 min and 103.5 min, respectively, with relative deviation of 6.8%. Considering the curves of accumulated gas volume flow and the trunk pipeline mid-point pressure with time, our results were in good agreement with the OLGA software simulation results. As for the curve of the venting riser outlet flow rate and the venting riser outlet pressure with time, the change trends of the proposed method and that of the OLGA software simulation were basically the same, but there was a certain difference between the results in the middle period. The reason for this may be that, when the OLGA software simulates the scenario, the logic for processing the boundary conditions of the venting riser outlet is different than that considered in this paper. In addition, the method for

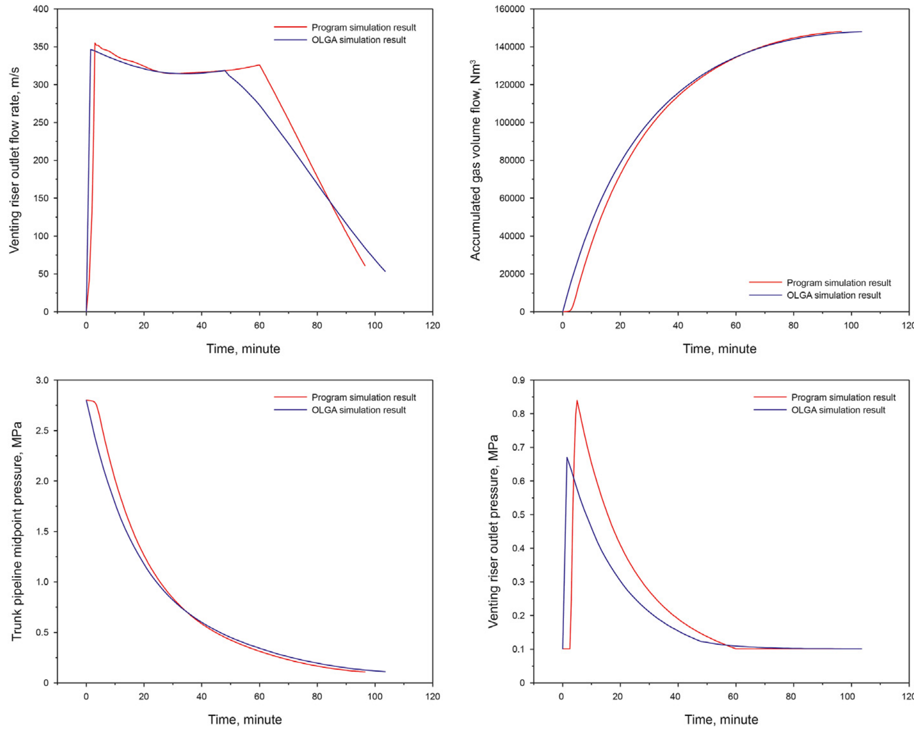

Fig. 5. Our simulation results and OLGA simulation results under the example conditions (the venting point is at one of the two ends).

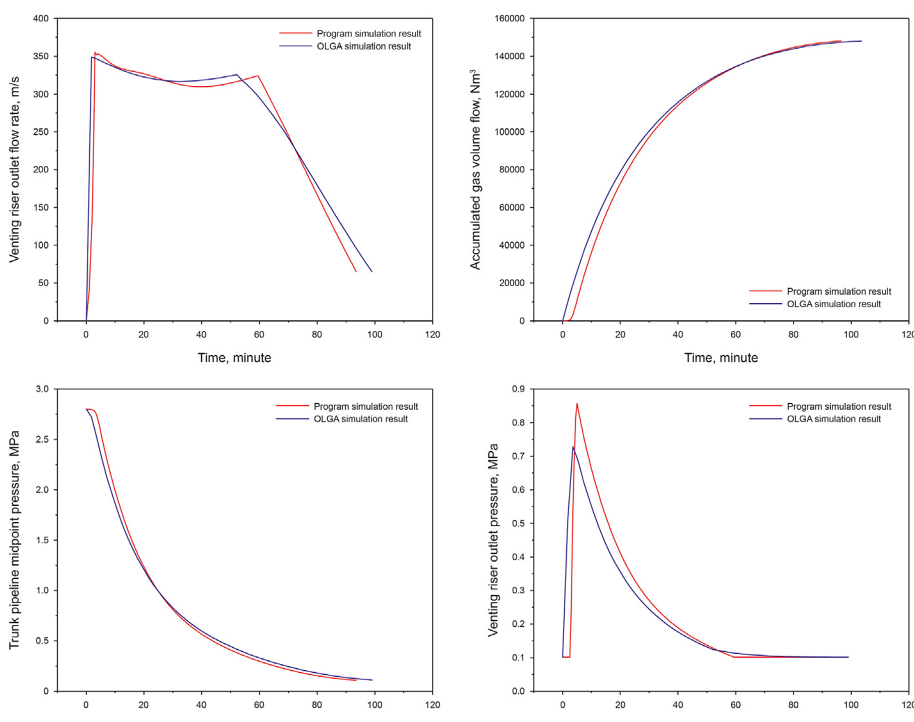

Fig. 6. Our simulation results and OLGA simulation results under the example conditions (the venting point is at the junction of two gas trunk pipeline segments).

determining the polytropic process index of the closed end in this paper was also inconsistent with that of the OLGA software, as it was found that the polytropic process index of the closed end in the OLGA simulation results changed with time. To a certain extent, the results obtained based on the two simulation methods were not completely consistent.

Based on the model shown in Fig. 3, it was assumed that the length of the upstream and downstream trunk pipeline segments bounded by the venting system pipeline was 8 km (the rest of the basic conditions were the same as Section 3.1). In this case, the proposed method's simulation results and those based on OLGA are shown in Fig. 6. The corresponding venting times for the two methods were 93.5 min and 99 min, respectively, with a relative deviation of 5.6%. In this venting scenario, the deviations in the flow rate and pressure at the outlet of the venting riser with time corresponding to the two simulation methods were similar to those observed in Fig. 5. The reason for this deviation may also be due to the boundary conditions for the closed end and the outlet of the venting riser under the two simulation methods being inconsistent. In OLGA, the boundary conditions at the outlet of the venting riser were the initial boundary conditions. However, during the venting process, the adjustment rules for the boundary conditions at the outlet of the venting riser are not yet clear. In the proposed model, the boundary condition of the outlet of the venting riser was set as a switching setting, considering the local speed of sound and atmospheric pressure.

Comparing the venting times for the corresponding examples in Figs. 5 and 6, we found that when the initial pressure, initial temperature, and total volume of natural gas of the gas trunk pipeline segment were the same, the venting time corresponding to the cases where the venting point is at the mid-point of the trunk pipeline segment and when the venting point was at one of the two ends were basically the same. It can be seen that, for the single-point venting of the horizontal trunk pipeline segment, when the other conditions are the same, the impact of the position of the venting point on the venting time is small.

In addition, by simulating multiple sets of examples, it was found that the venting time of the single-point venting scenario with the venting point at the junction of two gas trunk pipeline segments was slightly shorter (about 3% of the total venting time) than that where the venting point is located at one of the ends of the trunk pipeline segment, under the same basic conditions. To determine the reason why the venting was slightly faster in the former scenario, the pressure step method can be used for analysis:

The pressure variation range of the gas trunk pipeline segment during the whole venting process was divided into a series of depressurization intervals considering the micro-element pressure step size. For each micro-element de-pressurization interval, the endpoint pressure corresponds to the average pressure of the pipe section. Whether the venting point is at the junction of the two gas trunk pipeline segments or at one of the two ends of the trunk pipeline segment, the average venting flow (determined by time-based averaging) for each venting point in the depressurization interval is mainly determined by the average pressure in the depressurization interval; that is, the venting flow rate with the venting point at the junction is approximately equal to that when the venting point is at the end, and the total gas flow of the two venting scenarios is equal. The amount of natural gas venting corresponding to the same pressure reduction interval is fixed and, so, the venting time in the two venting scenarios is approximately equal. In addition, the gas at both ends of the trunk pipeline segment flows to the middle when the venting point is at the junction of the two gas trunk pipeline segments, while the gas flows from one side of the trunk pipeline segment to the other when the venting point is at one of the two ends of the trunk pipeline segment. From the viewpoint of flow friction, when considering the same depressurization interval, the gas corresponding to the depressurization interval with the venting point at the junction has a shorter flow distance and a smaller average friction loss, such that the average venting flow rate when the venting point is at the junction should be slightly higher than when the venting point is at the end (as shown in Fig. 7). Correspondingly, the venting time observed when the venting point was at the junction was slightly shorter than when the venting point was at the end.

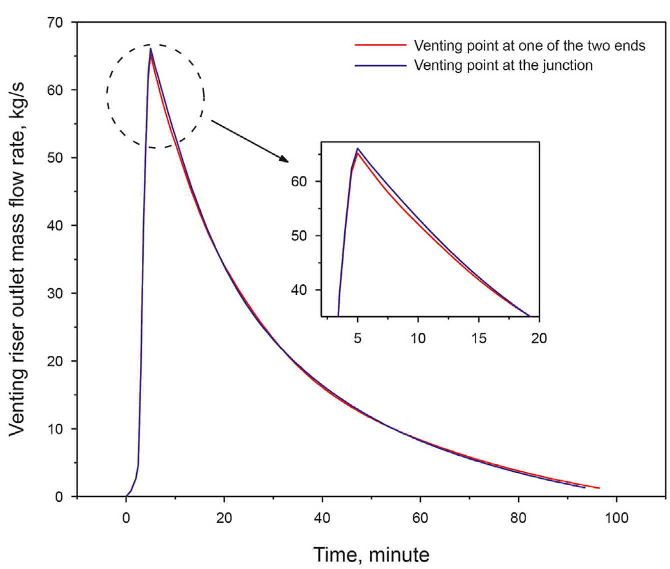

Fig. 7. Comparison of venting riser outlet mass flow rate between the two single-point venting scenarios.

The above calculation cases were all comparisons between the proposed model's results and those of OLGA. In order to further verify the accuracy of the established model, it was compared with actual on-site venting data. The results indicated that the error between the calculation results of the established model and the actual venting data was less than 10%. The calculation examples and comparison results are detailed in Table 4.

4. Venting valve opening control method

The venting valve is a key component in the venting system, and the valve opening scheme is an important factor affecting the venting time. Previous studies (Li et al., 2019; Bai et al., 2015; Zhang, 2021) have conducted simulation calculations by formulating a valve opening scheme in advance (e.g., opening the venting valve slowly and then quickly, opening the valve in multiple stages), and obtained the effect of the valve opening or the valve opening scheme on the venting time. It is considered that, during the venting process, by continuously adjusting the opening of the venting valve, the maximum instantaneous venting flow rate, the venting Mach number, and the noise and venting riser vibration generated during the venting process can be significantly reduced; however, in an actual venting scenario, due to the different venting processes, it is impossible to formulate a suitable valve opening scheme to meet all venting scenarios in advance. In addition, the staff at the scene generally control the venting process by observing the noise of the venting riser, the height of the venting flame, or the vibration of the venting pipe, and manually operating the venting valve by virtue of experience. As the staff at the scene cannot accurately understand the specific flow state of the gas during the venting process, and the formulation of a valve opening scheme lacks accurate judgment criteria, the valve opening scheme may be easily affected by the experience of the operator, the surrounding environment of the venting pipe, and other factors. In summary, the development of a venting valve adjustment method through formulating a valve opening scheme in advance or relying on operator experience has great limitations. Therefore, it is advisable to further study the opening control method of the venting valve during the venting process, in order to realize the flexible and precise adjustment of the venting valve in the venting process.

Table 4
Comparison of established model results with the actual venting data.

Number	Items	The vented pipe segment		
		SZ distribution station–HGT valve chamber	LZ valve chamber–H1 valve chamber	LQ distribution station–YCL distribution station
1	Diameter, mm	660	660	660
2	Pipe length, km	30.4	25	11.7
3	Pressure before venting, MPa	3.33	3.54	2.53
4	Pressure after venting, MPa	0.15	0.15	0.2
5	Venting point location	SZ distribution station, and HGT valve chamber	LZ valve chamber, and H1 valve chamber	LQ distribution station, and YCL distribution station
6	On-site emptying time, min	97	81	28
7	Established model emptying time, min	93	76	30.5
8	Relative error	4.1%	6.2%	8.9%

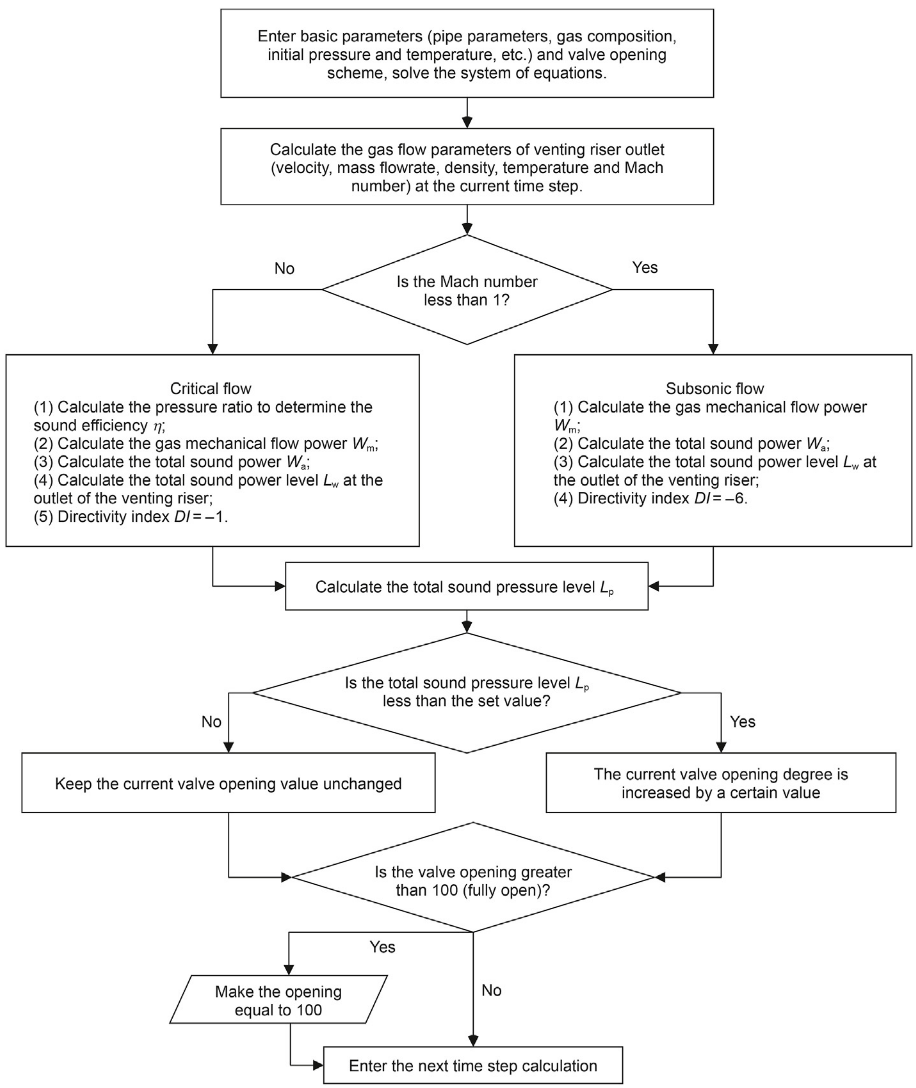

Fig. 8. Diagram of the valve opening control logic in the simulation program.

4.1. Control method

In view of the shortcomings of current venting valve control methods, based on the venting simulation model established in Section 2, a balance point for the valve opening was determined at each simulation time step, which can allow the venting operation to meet the requirements regarding noise (according to domestic relevant design requirements for the venting of the gas trunk pipeline segment, the maximum noise of continuous venting in a restricted area should not be higher than 85 dB (CDP-G-NGP-PR-102-2016-1, 2016)), as well as ensuring that the venting process is safe and stable. The specific idea is that, at each time step, according

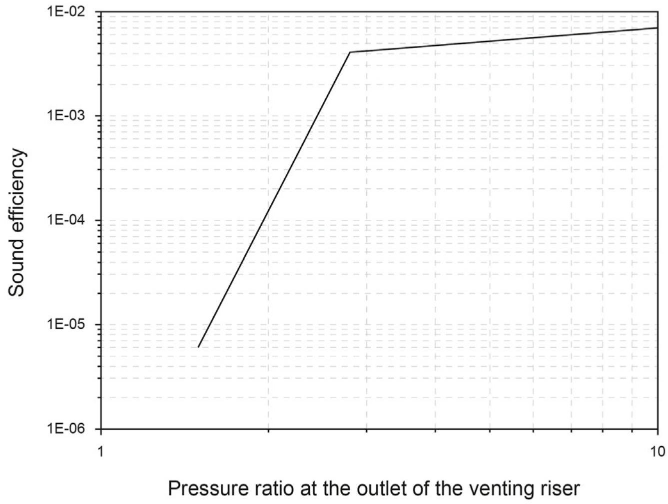

Fig. 9. Relationship between sound efficiency and pressure ratio at the outlet of the venting riser under critical flow discharge conditions.

to the flow parameters (i.e., gas flow velocity, Mach number, mass flow rate, and temperature) at the venting riser outlet, we calculate and judge whether the noise at the outlet of the venting riser at the current time step meets the required noise setting value (<85 dB). If the noise at the outlet of the venting riser at the current time step meets the requirement, the opening of venting valve will be automatically increased, according to a set adjustment amplitude value; if the noise does not meet the set value requirements, the opening of the venting valve will remain unchanged. The valve opening control logic in the simulation program is shown in Fig. 8.

Regarding Fig. 8, the noise calculation formula is shown in Eqs. 21–25. When the gas velocity at the venting riser outlet is subsonic, the jet noise is mainly turbulent noise, and there is an efficiency coefficient relationship between the sound power generated in the free space and the mechanical flow power, as shown in Eq. (21). The sound efficiency can be calculated using the empirical formula recommended by the API, as shown in Eq. (23), following which we can calculate the total sound power (Ma, 1983).

$$W_a = \eta W_{\mathrm{m}} \tag{21}$$

The mechanical power of the gas flow is equal to its convective

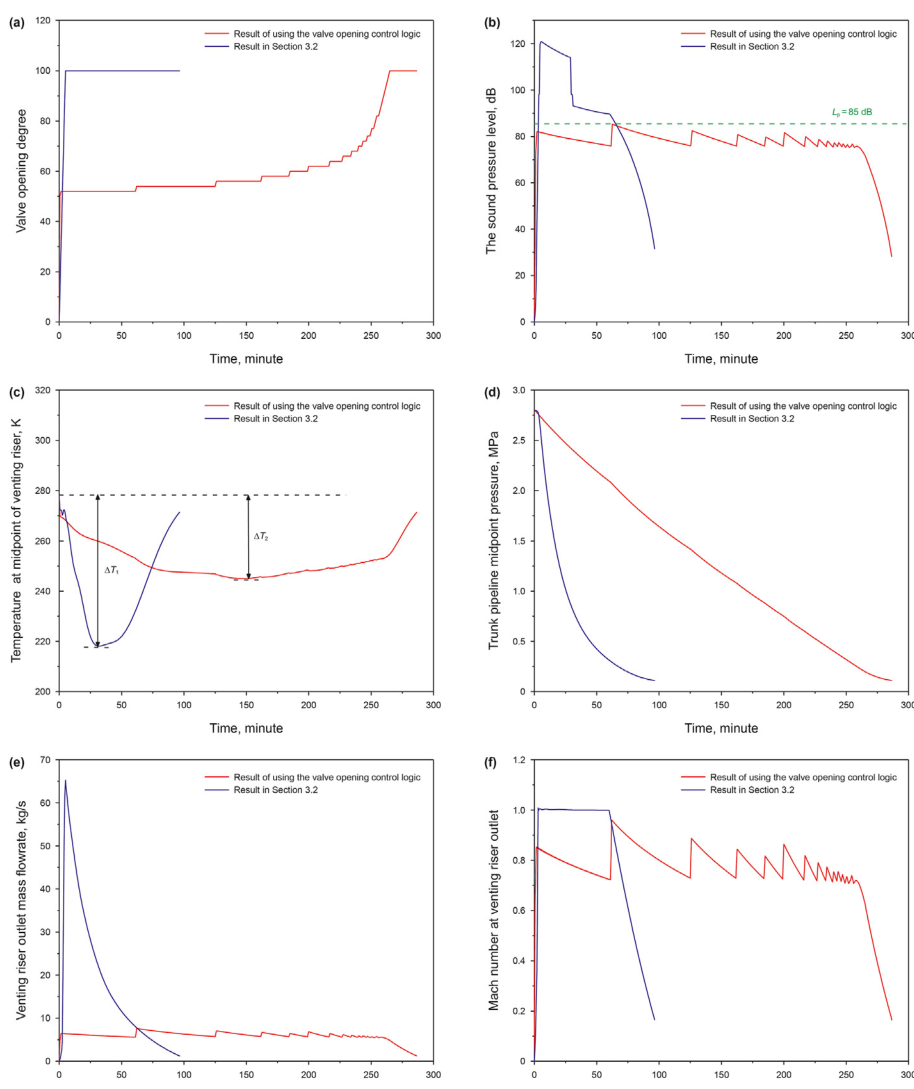

Fig. 10. Comparison between the results obtained using the valve opening control logic and the example results in Section 3.2.

energy when the cross-section is circular:

$$W_{\mathrm{m}}=\frac{\rho U^3\pi d^2}{8}=\frac{MU^2}{2} \tag{22}$$

For subsonic flow, the sound efficiency can be calculated using the following expression:

$$\eta=\left(\frac{T}{T_0}\right)^2\left(\frac{\rho}{\rho_0}\right)K_aMa^5 \tag{23}$$

When the gas velocity at the outlet of the venting riser is the critical speed of sound, there will be congestion and, in addition to the turbulent noise, the jet noise will also include shock noise. Meanwhile, the sound efficiency needs to be obtained, as shown in Fig. 9, and the total sound power is the sum of the turbulent sound power and the shock sound power, which can be calculated using Eq. (25).

The total sound power level of the gas flow at the outlet of the venting riser can be expressed as:

$$L_w=10\log_{10}W_a+120 \tag{24}$$

The total sound pressure level can be expressed as:

$$L_p=L_W+DI-10\log_{10}\left(4\pi r^2\right)W_a \tag{25}$$

4.2. Results comparison and discussion

Based on the model shown in Fig. 3, we took the initial valve opening as 50% (with the rest of the basic conditions as detailed in Section 3.1), the preset sound pressure as 80 dB, and the set adjustment amplitude value as 1%. A comparison between the results when using the valve opening control logic (shown in Fig. 8) and the example results in Section 3.2 is shown in Fig. 10.

According to the comparison between the results obtained using the valve opening control logic and the example results in Section 3.2, the analysis is as follows:

(1) As shown in Fig. 10(a), in the venting scheme regulated by the valve-opening control logic, the valve was opened in multiple stages during the venting process, where the valve-opening action was initially slow, then became fast. In this example, the cumulative venting time was 286.5 min, longer than the 96.5 min for the venting scheme in which the venting valve is opened linearly from 0% to 100% from 0 to 5 min (as described in Section 3.2).

(2) As shown in Fig. 10(b), in the venting scheme regulated by the valve-opening control logic, the total sound pressure at the outlet of the venting riser meets the specified requirements (<85 dB) during the entire venting process; while, in the example of Section 3.2, there was a period of time in which the specified maximum sound pressure (85 dB) was exceeded, which lasted for about 70 min; in particular, the maximum sound pressure reached 120 dB. The venting process regulated by the valve opening control logic avoids the noise problem existing in the traditional manual valve opening operations, thus reducing the adverse impact on the environment.

(3) As shown in Fig. 10(c), in the venting scheme regulated by the valve opening control logic, the maximum temperature drop of the venting riser was much lower than the maximum temperature drop corresponding to the valve opening scheme in Section 3.2. The venting scheme regulated by the valve opening control logic can avoid or reduce the occurrence of ice blockages in the venting pipe, thus protecting the venting pipe and related equipment.

(4) As shown in Fig. 10(d), in the venting scheme regulated by the valve opening control logic, the pressure drop rate in the gas trunk pipeline segment was more gradual than the corresponding pressure drop rate in Section 3.2, thus protecting the gas trunk pipeline segment.

(5) As shown in Fig. 10(e) and (f), in the venting scheme regulated by the valve opening control logic, the mass flow rate at the outlet of the venting riser was more stable (basically maintained in the range of 5–7 kg/s), the Mach number during the entire venting process was lower than 1, and the gas flow state in the entire venting process was subsonic flow, thus being more stable than the gas flow state corresponding to Section 3.2. The venting scheme regulated by the valve opening control logic, by adjusting the opening of the venting valve several times, reduces the maximum venting flow to the greatest extent, avoids or reduces vibration of the venting pipe, and protects the venting pipe and related equipment.

(6) The venting scheme regulated by valve opening control logic can be realized through the automatic control system of the station, avoiding the threat posed to the operator's health due to the noise and vibration generated during the venting process. In addition, in the venting scheme regulated by the valve opening control logic, the formulation of the valve opening scheme includes accurate judgment criteria (i.e., the venting simulation mathematical model, noise calculation algorithm, and valve opening control logic), and the valve opening scheme will not be affected by the surrounding environment of the venting pipe and other factors.

5. Conclusions

In this paper, based on two kinds of venting scenarios considering only one venting point in the venting system of a gas trunk pipeline segment, transient hydraulic–thermal simulation models were established to calculate the venting time of the gas trunk pipeline segment. Furthermore, based on this model, a method for venting valve opening control was proposed. The following conclusions can be drawn:

(1) Due to the short pipeline of the station venting system, when simulating the venting process of the gas trunk pipeline segment, in order to ensure the stability of the algorithm, it is recommended to use the implicit central difference method, which unconditionally satisfies the computational stability requirement. By increasing the calculation step, the calculation efficiency can be improved and the simulation time can be shortened. For example, according to the basic conditions of the calculation example detailed in Section 3.1, with little difference in the calculation results of the venting time, when the time step is 30 s, the calculation time is 675.2 s and, when the time step is 60 s, the calculation time is 364.6 s.

(2) In order to ensure that the mathematical equations of the venting simulation model are closed, two boundary conditions need to be set at the closed end of the gas trunk pipeline segment. In addition, as the gas flow velocity at the outlet of the venting riser cannot be higher than the speed of sound, it is necessary to consider switching of the pressure and speed of sound boundary conditions at the outlet of the venting riser.

(3) For the single-point venting of a horizontal gas trunk pipeline segment, under the same basic conditions, the impact of

the venting point position on the venting time is small. In addition, under the same basic conditions, the venting time obtained when the venting point is at the junction of two gas trunk pipeline segments is slightly shorter (about 3% of the total venting time) than when the venting point is located at one of the ends of the trunk pipeline segment.

(4) In the venting scheme regulated by the valve opening control logic, during the venting process, the opening of the venting valve is automatically adjusted according to the flow state of the venting gas, allowing for minimization of the maximum venting flow, the maximum temperature drop of the venting riser, and the sound pressure at the outlet of the venting riser; in this example, the maximum sound pressure at the outlet of the riser was reduced by 32%, the maximum temperature drop of the riser was reduced by 45%, and negative effects such as vibration, noise, ice blockage, and so on were avoided, improving the safety of the venting process.

Declaration of competing interest

The authors declare that they have no known competing financial interests or personal relationships that could have appeared to influence the work reported in this paper.

Acknowledgement

The work is supported by the National Natural Science Foundation of China (Grant No. 52174064).

References

Bai, X., Li, Z.L., Jiang, H.B., Al, E., 2015. Development of software for calculating venting volume of venting system in gas transmission trunk line[J]. Natural Gas and Oil 33 (6), 11–15 (**in Chinese**). https://10.3969/j.issn.1006-5539.2015.06.003.

CDP-G-NGP-PR-102-2016-1, 2017. Guidelines for Calculation of Vent in Gas Pipeline Engineering[S] (**in Chinese**).

Chaczykowski, M., Zarodkiewicz, P., 2017. Simulation of natural gas quality distribution for pipeline systems. Energy 134, 681–698. https://doi.org/10.1016/j.energy.2017.06.020.

Chen, Q., Wu, C.C., Zuo, L.L., Mehrtash, M., Wang, Y.X., Bu, Y.R., Sadiq, R., Cao, Y.K., 2021. Multi-objective transient peak shaving optimization of a gas pipeline system under demand uncertainty. Comput. Chem. Eng. 147, 107260. https://doi.org/10.1016/j.compchemeng.2021.107260.

Chen, Q., Xing, X.K., Jin, C., Zuo, L.L., Wu, J.H., Wang, W.S., 2020. A novel method for transient leakage flow rate calculation of gas transmission pipelines. J. Nat. Gas Sci. Eng. 77, 103261. https://doi.org/10.1016/j.jngse.2020.103261.

Elaoud, S., Hafsi, Z., Hadj-Taieb, L., 2017. Numerical modelling of hydrogen-natural gas mixtures flows in looped networks. J. Petrol. Sci. Eng. 159, 532–541. https://doi.org/10.1016/j.petrol.2017.09.063.

Ettouney, R.S., El-Rifai, M.A., Elzoubier, A.A., 2012. Emergency venting into redundant pipelines. J. Loss Prevent. Proc. 25 (4), 739–745. https://doi.org/10.1016/j.jlp.2012.04.009.

Helgaker, J.F., Müller, B., Ytrehus, T., 2014. Transient flow in natural gas pipelines using implicit finite difference schemes. J. Offshore Mech. Arctic Eng. 136 (3). https://doi.org/10.1115/1.4026848.

Jia, B.Y., Wang, H., Lin, C., 2016. Dynamic simulation and analysis on nature gas pipeline blowdown process[J]. Chem. Eng. Oil Gas 45 (6), 18–20 (**in Chinese**). https://10.3969/j.issn.1007-3426.2016.06.005.

Li, C.J., Huang, Z.J., 2016. Natural Gas Pipeline transportation[M]. Petroleum Industry Press, BeiJing (**in Chinese**).

Li, Y.T., Ji, Z.L., Yu, Y., Al, E., 2018. Discharge effect analysis and improvement of the venting system of large diameter and high pressure gas line pipes[J]. Nat. Gas. Ind. 38 (2), 97–102. https://doi.org/10.3787/j.issn.1000-0976.2018.02.013 (**in Chinese**).

Li, Y.T., Wu, C.C., Lei, Y.T., Al, E., 2019. Comparison analysis on the scheduled venting modes of gas pipelines[J]. Oil Gas Storage Transp. 38 (4), 429–434. https://doi.org/10.6047/j.issn.1000-8241.2019.04.012 (**in Chinese**).

Lin, Q., Lou, C., Gong, J., Al, E., 2019. Venting operation hydraulic calculation research of gas transmission truck line and station based on C language[J]. Gasf. Surf. Eng. 38 (S1), 36–41. https://doi.org/10.3969/j.issn.1006-6896.2019.z1.008 (**in Chinese**).

Liu, G.W., Wang, X.W., 2015. Analysis of emptying process of gas transmission pipeline[J]. Gas Heat 35 (6), 38–40. https://doi.org/10.3969/j.issn.1000-4416.2015.06.022 (**in Chinese**).

Liu, Y.N., Zhang, X., Shan, L., 2014. Calculation of venting time of natural gas pipeline based on characteristic linemethod[J]. Oil Gas Storage Transp. 33 (12), 1338–1342. https://doi.org/10.6047/j.issn.1000-8241.2014.12.017 (**in Chinese**).

Lou, C., Gong, J., Lin, Q., Al, E., 2014. Hydraulic characteristics of venting system in gas transmission trunk line [J]. Oil Gas Storage Transp. 33 (5), 542–548. https://doi.org/10.6047/j.issn.1000-8241.2014.05.019 (**in Chinese**).

Ma, D., 1983. Acoustics manual[M]. Science Press, BeiJing (**in Chinese**).

Meng, Y.Z., Chen, R.R., Deng, T.H., 2022. Two-stage robust optimization of power cost minimization problem in gunbarrel natural gas networks by approximate dynamic programming. Petrol. Sci. https://doi.org/10.1016/j.petsci.2021.09.048.

Pei, N., Zhao, L.H., Cao, S.R., 2014. Research on vent control of natural gas pipelines and stations[J]. Journal of Petroleum and Natural Gas 36 (8X), 3 (**in Chinese**).

Pu, L.Z., Chen, L.Q., Yang, W.C., 2014. Setting of nature gas ventpipe[J]. Natural Gas and Oil 32 (1), 3. https://doi.org/10.3969/j.issn.1006-5539.2014.01.014 (**in Chinese**).

Qiao, Z.F., Guo, Q.H., An, J.F., 2013. Simulation analysis of venting pipeline of high-pressure natural gas pipeline[J]. Gas Heat 33 (4), 30–33. https://doi.org/10.3969/j.issn.1000-4416.2013.04.008 (**in Chinese**).

Sichuan Petroleum Design Institute, 1974. Gas Trunk Pipeline Segment Design Manual [S] (**in Chinese**).

Sichuan Petroleum Administration, Southwest Petroleum Institute, 1995. Long-distance Pipeline Design and construction[M]. Petroleum Industry Press (**in Chinese**).

Soltanieh, M., Zohrabian, A., Gholipour, M.J., Kalnay, E., 2016. A review of global gas flaring and venting and impact on the environment: case study of Iran. Int J. Greenh Gas Con 49, 488–509. https://doi.org/10.1016/j.ijggc.2016.02.010.

Su, H., Zio, E., Zhang, Z.J., Xiong, C.Z., Dai, Q.S., Wu, Q.W., Zhang, J.J., 2022. Development of an integrated dynamic model for supply security and resilience analysis of natural gas pipeline network systems. Petrol. Sci. 19 (2), 761–773. https://doi.org/10.1016/j.petsci.2021.10.002.

Wei, F.L., Liu, J.L., Yuan, H.R., 2021. Global stability to steady supersonic solutions of the 1-d compressible euler equations with frictions. J. Math. Anal. Appl. 495 (2), 124761. https://doi.org/10.1016/j.jmaa.2020.124761.

Xiong, Y., Zhang, L.P., Zhu, T.T., 2014. Research of emergency venting time in natural gas pipeline accidents with sps. Procedia Eng. 84, 927–932. https://doi.org/10.1016/j.proeng.2014.10.517.

Zhang, G.Z., 1994. Pipeline Transient Flow analysis[M]. Petroleum University Press (**in Chinese**).

Zhang, K., 2021. Calculating venting time of gas pipelines and operation control methods[J]. Natural Gas Technology and Economics 15 (2), 27–32. https://doi.org/10.3969/j.issn.2095-1132.2021.02.006 (**in Chinese**).

Zhu, Y.Q., Wang, P., Wang, Y., Tong, R.K., Yu, B., Qu, Z.G., 2021. Assessment method for gas supply reliability of natural gas pipeline networks considering failure and repair. J. Nat. Gas Sci. Eng. 88, 103817. https://doi.org/10.1016/j.jngse.2021.103817.

Zuo, L.L., Jiang, F., Jin, B., Zhang, L., Xue, T., 2015. Value setting for the rate of pressure drop of automatic line-break control valves in natural gas pipelines. J. Nat. Gas Sci. Eng. 26, 803–809. https://doi.org/10.1016/j.jngse.2015.07.002.